Fe₃O₄ Nanoparticles Capped with PEG Induce Apoptosis in Breast Cancer AMJ13 Cells Via Mitochondrial Damage and Reduction of NF-κB Translocation

Majid S. Jabir, Uday M. Nayef, Waleed K. Abdulkadhim, Zainab J. Taqi, Ghassan M. Sulaiman, Usama I. Sahib, Ahmed M. Al-Shammari, et al.

ONLINE FIRST

Springer

Springer

Fe$_3$O$_4$ Nanoparticles Capped with PEG Induce Apoptosis in Breast Cancer AMJ13 Cells Via Mitochondrial Damage and Reduction of NF-κB Translocation

Majid S. Jabir[1] · **Uday M. Nayef**[1] · **Waleed K. Abdulkadhim**[1] · **Zainab J. Taqi**[1] · **Ghassan M. Sulaiman**[1] · **Usama I. Sahib**[1] · **Ahmed M. Al-Shammari**[2] · **Yu-Jen Wu**[3] · **Mohamed El-Shazly**[4,5] · **Ching-Chyuan Su**[6]

Abstract

In the current study, polyethylene glycol (PEG) was employed to cap super magnetite nanoparticles (Fe$_3$O$_4$ NPs) through hydrothermal preparation. The main goal of this study is to investigate the influence of physical incorporation of polyethylene glycol (PEG) loaded Fe$_3$O$_4$. The anticancer potentials of these particles were studied against breast cancer cell line (AMJ13). Syntheses bare Fe$_3$O$_4$, and Fe$_3$O$_4$-PEG were confirmed by TEM, SEM, and FTIR. The size of Fe$_3$O$_4$ nanoparticles range of 9–20 and 5–12 nm for the Fe$_3$O$_4$–PEG nanoparticles which exerted superparamagnetic properties as well as elevated saturation level of magnetization at ambient conditions. The MTT test was employed to detect the ability of the bare Fe$_3$O$_4$ and Fe3O4-PEG on the proliferative of AMJ13 cells. IC$_{50}$ values was 37.33 μg mL^{-1} for bare Fe$_3$O$_4$ and 18.23 μg mL^{-1} for Fe$_3$O$_4$-PEG. AMJ13 Cells exposed to bare Fe$_3$O$_4$, and Fe$_3$O$_4$-PEG NPs demonstrated a significant cell death, which increased with PEG, loaded Fe$_3$O$_4$ NPs. The capability of Fe$_3$O$_4$-PEG to induce cellular apoptosis was tested using DAPI, Acridine orange/ Ethedium bromide stains, flow cytometry, with the assays of mitochondrial membrane potential (MMP), and the production of reactive oxygen species (ROS). RT-PCR, and immunofluorescence were performed to measure expression levels of Bax and Bcl-2 proteins. The toxicity of bare Fe$_3$O$_4$ and Fe$_3$O$_4$-PEG nanoparticles using animal model were investigated. Animal's body weight, liver and kidney function enzymes, and histological alterations for liver, kidney, and lungs were addressed. The findings demonstrated that nanoparticles were biocompatible with liver and kidney function enzymes and no significant alterations were recorded in the liver, kidney and the lungs. Both nanoparticles revealed a proliferation inhibitory effect on AMJ13 cells, resulting in apoptosis as a novel pathway that involve the mitochondrial damage and NF-kB. Taken together the present data suggest that bare Fe$_3$O$_4$ and Fe$_3$O$_4$-PEG could be promising therapy protocol for cancer cells.

Keywords Fe$_3$O$_4$ · Fe$_3$O$_4$-PEG · Anticancer activity · AMJ13 cells · Mitochondrial damage · NF-kB pathway

✉ Majid S. Jabir
100131@uotechnology.edu.iq

✉ Yu-Jen Wu
x00002180@meiho.edu.tw

✉ Ching-Chyuan Su
a085085@mail.tsmh.org.tw

1 Applied Science Department, University of Technology, Baghdad, Iraq

2 Iraqi Center for Cancer and Medical Genetic Research, University of Mustansiriyah, Baghdad, Iraq

3 Department of Beauty Science, Meiho University, 91202 Pingtung, Taiwan

4 Department of Pharmaceutical Biology, Faculty of Pharmacy and Biotechnology, German University in Cairo, 11835 Cairo, Egypt

5 Department of Pharmacognosy, Faculty of Pharmacy, Ain-Shams University, Abassia, 11566 Cairo, Egypt

6 Antai Medical Care Corporation Antai Tian-Sheng Memorial Hospital, 928 Pingtung, Taiwan

1 Introduction

Being among the top health threats in the 21st century, cancer is a lethal disease with no geographical or organ limitations that cause worldwide annual mortality that exceeds 12.7 million people [1]. Among women, breast cancer is responsible for 16% of the entire cancer cases, and about 23% of invasive types, being the most widely prevailed invasive cancer among women. Cancer originates from mutated growth-controlling genes that are involved in DNA repair as well as cell division and death. Cancer can occur accidentally when a portion of the genetic code is miscopied, while DNA damage caused by chemical, viral, or radiation exposure might lead to environmentally mediated cancer induction [2].

Fe_3O_4 nanoparticles are characterized by their dual diagnostic and therapeutic advantages, their high contrasting properties during magnetic resonance imaging tests, and their hyperthermic properties (40–43 ℃) which is sufficient to kill many cancer cells [3]. The uniqueness of these nanoparticles is ensured by their highly effective tracing and, subsequently, killing potentials of cancer cells. It is also possible to use heating systems that are dependent on Fe_3O_4 to regulate the liberation of drugs from their delivery system. Such systems are set up so they liberate their content at specific temperatures, bringing up more advantages from the combined use of the NPs-dependent delivery system and hyperthermia modality for the treatment of cancer [4]. Hyperthermia is applied to malignant tissues by following two main approaches; first, extracellular hyperthermia involves the use of an outer heat source such as a water bath, microwave, ultrasound, and infrared sauna. Second, intracellular hyperthermia which involves the use of the alternating current field to heat the tumor tissue mass through Fe_3O_4 NPs that are already inserted into the cancer cells [5]. Nevertheless, it is yet unknown how the photothermal impact provided by the magnetized Fe_3O_4 NPs exerts its influence on cancer cells or tumor mass. Extensive investigation has been carried out to clarify the biochemical pathways associated with the use of Fe_3O_4-PEG NPs in cancer therapy [6].

Mg is essential for humans and its alloys are frequently used in biometallic implants. Mg/Au or Mg/Pt Janus micromotors have exhibited motions in chloride and bicarbonate ion solutions through continuous Mg-water reaction via the removal of Mg(OH)2 passivation layer by these.

ions. These laid the foundation for biocompatible chemically- powered micromotors. Subsequently, Mg/Pt-PNIPAM Janus micromotors showed capacity for moving in human.

blood plasma and temperature controlled drug delivery that open doors for implementing real application in the

human body. Recently, Mg-based micromotors exhibited motion and drug delivery capabilities in mouse intestine and stomach which provided a further step toward use in whole organisms. Mg/Pt Janus micromotors had cytotoxic effect against different cancer cell lines such as human lung carcinoma epithelial cells (A549), human breast cancer cells.

(MCF-7), human embryonic kidney cells (HEK-293), human liver carcinoma cells (HepG2) and human cervical cancer cells (HeLa) after incubating at different concentrations for 24 hours [7]. Superparamagnetic iron oxide (Fe3O4) NPs are traditional T2-weighted contrast agents, of which the r2 values are related to their sizes and aggregation states. Fe3O4 nanoparticles coassembly with polymer-tethered Au NPs, and free amphiphilic block copolymers into Janus hybrid vesicles. In the vesicles, the assembly of Fe3O4 NPs and aggregation of Au NPs into half of the vesicles with enhanced plasmon coupling led to 4 times enhancement of r2 values than individual Fe3O4 NPs and strong absorption in the NIR range, respectively. After intravenous injection, the accumulation of vesicles in tumours could be enhanced by applying an external magnet close to tumours and monitored through MRI and PAI [8]. Recent studies demonstrated the important of concentration of nanomaterials and optical properties for improve the applications of these nanomaterials in photo –catalysis [9, 10], In addition, the photocatalytic activities of the composites nanoparticles samples were studied based on the degradation of methylene blue (MB) as a model compound, where the results illustrated that the α-Fe2O3@50% TiO2 nanocomposites performed the best as a photocatalyst under visible light. These nanocomposites samples provide a positive example for the fabrication of other structures for photocatalysis or other applications. [11].

Apoptosis is a critically important cellular homeostatic regulation mechanism for controlling the population size of various cell types [12]. Such a mechanism of programmed cell death gained significant interest from investigators due to the high level of resemblance between this natural cell death pathway and the artificial anti-cancer drugs in terms of their modes of action [13]. The formation of ROS in high levels within cancer cells is a critical event for induction of apoptosis [14], as it results in a sequence of reactions that involve DNA oxidative damage, MMP disruption, cytochrome c release, and eventually the induction of the caspase chain reactions [15]. Furthermore, the disturbance in the expression levels of Bcl-2 and Bax proteins has a critical influence on the extent of cancer cell susceptibility to therapeutic drugs [16]. Published studies on the anti-tumor treatment protocols revealed that the continual induction of NF-κB (nuclear factor-kappa B) influences the tumor development process [17]. Thus, the active induction of apoptosis in cancer cells can be achieved using anti-cancer drugs with

the ability to suppress intracellular translocation of NF-κB. Nevertheless, there is an overgrowing necessity to develop new and more active antitumor therapies.

Data on physiological and cellular levels as related to the modes of interaction between novel NPs and tumor cells are rare in general. Once capped, the inherent physical and chemical features of the surface of NPs, such as surface functionality, charge, reactivity, and dimension are altered, providing them with higher degrees of stability and suitability for the in vitro uses. Coating substances such as PEG can be used to prepare the hydrophilic surface of Fe_3O_4 NPs. Previous studies tested the use of AFM to induce the heating behavior of Fe_3O_4 NPs and the efficiency of these particles in killing ovarian cancer cells [18]. The photothermal effect of Fe_3O_4 and Fe_3O_4-PEG core-shell nanoparticles for killing bacteria and cancer cell lines was recently reported [6]. This study aimed to prepare Fe_3O_4 nanoparticles capped with PEG and to investigate how these nanoparticles affect breast cancer cells AMJ13 and the possible mechanisms involved in this effect.

2 Materials and methods

2.1 Chemicals

Ferric chloride hexahydrate ($FeCl_3 \cdot 6H_2O$), ethylene glycol (EG), anhydrous sodium acetate (NaOAc), ethanol, polyethylene glycol (PEG-4000), and ethanolamine (ETA) were purchased from (Gainland chemicals company, U.K).

2.2 Preparation of bare Fe_3O_4 magnetic NPs

Fe_3O_4 NPs were prepared using the hydrothermal approach. Accordingly, 1.5 gm of $FeCl_3 \cdot 6H_2O$ was dissolved in 40 mL solvent containing ETA (20 mL) and EG (20 mL), until the development of a stable orange solution. NaOAc (4.0 g) was mixed with the solution which was homogenized using a magnetic stirrer and heated in a sealed autoclave at 200 °C. Following 10 h reaction time, the autoclave was brought to ambient temperature, and the magnetic NPs were sequentially washed with absolute ethanol and deionized water before an overnight drying step at 60 °C.

2.3 Characterization of bare Fe_3O_4 and Fe_3O_4-PEG

Morphological properties of the prepared MNPs were studied by employing scanning (TESCAN, Vega III, Czech Republic) and transmission electron microscopy (TEM; Philips). The preparation of the samples for the transmission electron microscope test was performed by adding one drop of the MNPs solution onto a 200-meshed gold-coated copper grid. The structural properties of the prepared magnetite nanoparticles (MNPs) were investigated using FTIR.

2.4 MTT assay

This test was conducted as previously described [19]. In brief, seeding of the tested cells (1×10^5 cells mL^{-1}) was performed in 96 well microtiter plates that contain a mixture of RPMI medium and fetal calf serum (10%). Overnight incubation of the cells was performed for attachment followed by the treatment with bare Fe_3O_4 and Fe_3O_4-PEG, and another incubation for 72 h. Further treatment included washing with phosphate-buffered saline for 3 times, staining with MTT (2 mg mL^{-1}), the incubation (3 h, 37 °C), and treatment with DMSO. Next, a microplate reader was employed to measure the absorbance (420 nm). Finally, the growth inhibition rate (cytotoxicity in %) was determined via the equation below:

$$\text{Inhibition rate\%} = (A - B/A) \times 100 \tag{1}$$

where A and B are optical densities for the control and the treated sample, respectively [20].

2.5 Acridine Orange–Ethidium Bromide (AO/EtBr) Dual Staining

The (AO/EtBr) double staining method was conducted based on previously published protocols. Briefly, the bare Fe_3O_4 and Fe_3O_4-PEG (9.23 and 57.55 μg mL^{-1}, respectively) were used to treat the cells within 96-well plates. After incubation (24 h) and washing 2 times with phosphate-buffered saline, they were mixed with 100 μL of AO/EtBr for 1 min. Finally, the cells were visualized under fluorescence microscopy [21].

2.6 Assessment of Apoptosis Using DAPI Stain

AMJ13 cells were examined under the fluorescence microscope after they were subjected to the DAPI stain. Seeding of the cells (5×10^3) was achieved by adherence to sterile coverslips placed at the bottom of 6-well plates (48 h, 5% CO2, 95% air, 37 °C). Then AMJ13 cells were treated (24 h) with bare Fe_3O_4 and Fe_3O_4-PEG (9.23 and 57.55 μg mL^{-1}, respectively). The medium was discarded, filtered phosphate-buffered saline was used to wash the cells, which were then fixed with 96% ethanol (0.5-1 h). After the removal of the fixative, another washing step was performed with distilled water, followed by staining with DAPI (0.5-1 h). After DAPI removal from the coverslips, they were subjected to washing with distilled water followed by air drying and mounting on a glass slide. A fluorescence microscope

(40X) was finally used to examine the morphological properties of the cells [22].

2.7 Flow Cytometry

The detection of apoptosis using flow cytometry assay was done according to the previous study. In brief, AMJ13 cells treated with Fe_3O_4 and Fe_3O_4-PEG were analyzed by determining the ratio of cells with nucleus concentration and fragment. AMJ13 cells were seeded for 24 h then treated with Fe_3O_4 and Fe_3O_4-PEG at IC_{50} concentration. Cells were suspended in the FACS buffer. Then, all treated and non-treated cancer cells were stained with PI, and annexin V-FITC (Invitrogen, Carlsbad, CA) and measured to investigate the apoptotic cells using flow cytometer assay [23].

2.8 Mitochondrial membrane potential

For the simultaneous assessment of the critical apoptosis events in AMJ13 cells following treatment with Fe_3O_4 and Fe_3O_4-PEG, Cellomics Multiparameter Cytotoxicity 3 Kit (ThermoScientific™, Pittsburgh, PA, USA) was employed. In brief, seeding of AMJ13 cells was performed into 96-well plates (24 h), followed by treatment with bare Fe_3O_4 and Fe_3O_4-PEG at concentration IC_{50} (18.23 μg mL^{-1} and 37.33 μg mL^{-1}, respectively). The cells were then stained with cell permeability and MMP stains. To confirm the critical apoptotic events in the AMJ13 cells treated with Fe_3O_4 and Fe_3O_4-PEG, Rh123 a fluorescent dye repossessed by lively mitochondria without cytotoxic effects. This dye is used to investigate the membrane potential of the mitochondrial cells before and after the treatment with bare Fe_3O_4 and Fe_3O_4-PEG nanoparticles. In brief, 24 h seeding of cells in 96-well plates was followed by the treatment with the IC_{50} dose of Fe_3O_4 and Fe_3O_4-PEG and staining with Rh123 dyes at concentration 1 M for 2 h at 37 °C. The cells were detached by 0.5% trypsin-EDTA then centrifuged at 400 rpm for 5 minutes. Cells were suspended in FACS buffer and measured by flow cytometry assay, and histograms were made.

2.9 Localization of Fe_3O_4 and Fe_3O_4-PEG in Treated AMJ13 Cells

Fe_3O_4 and Fe_3O_4-PEG nanoparticles labeled with a fluorescent stain. In brief, FITC (Sigma-Aldrich, USA) at concentration 1 mg mL^{-1} was mixed with Fe_3O_4 and Fe_3O_4-PEG at IC_{50} concentration, followed by incubation at room temperature for 10 h in the dark. The reaction was satisfied using the Tris buffer (pH 10). FITC-labeled nanoparticles were collected by centrifugation and washed twice with DMSO to remove unbound FITC. The FITC-labeled nanoparticles suspension was added to AMJ13 cells. Then, the mixtures

were incubated for 24 h at 37 °C. Cells were washed. DAPI stain was used to stain the nuclei. The images were taken by a fluorescent microscope.

2.10 ROS Generation Assay

The breast cancer cells (AMJ13) were seeded at a concentration of 1×10^5 cells/well in the complete growth medium. Then, the cells were treated for 24 h with bare Fe_3O_4 and Fe_3O_4-PEG (9.23 and 57.55 μg mL^{-1}, respectively), resuspended in H2DCFDA dye (10 μM), and incubated at 37 °C for 10–30 minutes. After removal of the loading buffer, the cells were washed for 3 times with pre-warmed buffer (HBSS, or HEPES) and returned to incubation with pre-warmed growth medium (37 °C, 10–20 min) to induce the hydrolysis of intracellular acetate groups by esterase enzymes and, eventually, ensure responsiveness of the dye to oxidation. Cells were immediately examined with a fluorescence microscope with 488 nm excitation using an emission filter appropriate for fluorescein [24].

2.11 RT-PCR

Bax and Bcl-2 protein expression levels in the treated AMJ13 cells were determined using RT-PCR. Isolation of the total RNA in the cells was performed using an RNeasy Mini kit by following the protocol provided by the supplier (Qiagen. Cat. No.74,104, UK). DNAse I was used to treating RNA and the product was employed to synthesize cDNA with the enzymatic reaction of superscript II reverse transcriptase (Invitrogen. Cat. No. 18064-071, USA) based on the supplier's procedure. Fast SYBR Green PCR master mix (Applied Biosystems. Cat. No. 4,385,612, UK) was employed with a 7900HT fast system (Applied Biosystems) to conduct the quantitative reverse transcription PCR (q RTPCR). Normalization of gene expression levels was performed to TATA-binding protein (TBP). Calculation of the mean relative gene expression was achieved following Livak's method. All tests were conducted in triplicate [25].

2.12 Immunofluorescence microscopy

AMJ13 cells were treated with bare Fe_3O_4 and Fe_3O_4-PEG at concentrations of 9 0.23 and 57.55 μg mL^{-1}, respectively, followed by washing for 3 times with phosphate-buffered saline, fixation in 2% PFA (30 min, 20 °C), permeabilization with 0.3% Triton-X (30 min, RT), and blocking in 5% normal goat serum (1 h). Bax and Bcl-2 primary Abs (1 μg mL^{-1}) were applied to the cells (2 h, RT) and then washed out before applying the secondary Ab (1 h, RT). The Abs used were goat anti-rabbit IgG (1 μg mL^{-1}) coupled to Alexa Fluor 488 fluorescent dye. After washing with phosphate-buffered saline, the stained cells were mounted in a Vecta

shield with DAPI, followed by viewing with a Meta confocal microscope (LSM 510) [26].

2.13 Measurement of NF-κB Activity

AMJ13 cells (1.0×10^4 cells well^{-1}) were treated with bare Fe_3O_4 and Fe_3O_4-PEG at concentrations of 9.23 and 57.55 μg mL^{-1}, respectively, for 12 h. Thirty minutes treatment with TNF-α (5 ng mL^{-1}) was applied to stimulate the treated cells, followed by fixation, permeabilization and blocking with 5% normal goat serum. NF-κB primary Ab (1 μg mL^{-1}) was applied to the cells (2 h, RT), followed by washing and application of the secondary Ab (1 h, RT). The Abs used were goat anti-rabbit IgG (1 μg mL^{-1}) coupled to Alexa Fluor 488 fluorescent dye. After washing with phosphate-buffered saline, the stained cells were mounted in a Vecta shield with DAPI, followed by viewing with a Meta confocal microscope (LSM 510) [27].

2.14 Toxicity of Fe₃O₄ and Fe₃O₄-PEG on Human Blood Components

Blood samples were obtained from healthy volunteers based on the method of National Institute of Health and Food and Drug Administration and as per the declaration and regulation of Helsinki of 1975 as a statement of ethical principles. Permission was obtained from the hospitals of the medical city in Baghdad, Iraq and approved by the institutional ethical committee of university of technology, Baghdad, Iraq (Ref. No. AS 407-23-09-2017). The study participants were informed about the value of the study before we are gaining to collect any data or samples. Informed consent and/ or assent were obtained from the study participants. Fe_3O_4 and Fe_3O_4-PEG at concentration 10 μg/mL, was added to blood samples. After 60 min of incubation at 37 °C. Then, the blood components were measured [28].

2.15 A Study of Magnetic NPs Toxicity Using an Animal Model

Balb /c mice (20–30 g weight, 6–8 weeks old) were obtained from the Iraqi Center for Cancer and Medical Genetic Researches, the University of Al-Mustansiriyah, Baghdad, Iraq. were acquired and kept in an isolated animal facility with sufficient access to water and food. All procedures were performed under the U.S. National Institutes of Health (NIH) Guide for the Care and Use of Laboratory Animals (NIH Publication No. 86-23, revised in 1996) and were approved by Animal Care and Ethics Committee at Biotechnology Division, Applied Sciences Department, University of Technology, Baghdad, Iraq (Ref. No. AS 407-23-09-2017). Mice were divided into 9 random groups, each with 3 mice: Group 1 received intraperitoneal injections of phosphate-buffered saline (250 μL) and served as the control group. Groups 2, 3, 4, and 5 received intraperitoneal injections of 500 μg kg^{-1} Fe_3O_4 for 1, 2, 3, and 4 weeks, respectively. Groups 6, 7, 8, and 9 received intraperitoneal injections of 500 μg kg^{-1} Fe_3O_4-PEG for 1, 2, 3, and 4 weeks, respectively. At the end of the fourth week, an anesthetization of the mice was performed using sodium pentobarbital, followed by blood collection and serum isolation based on standard procedures. Tissues from the liver, kidneys, and lungs were collected and subjected to standard fixation and staining protocols before being tested under optical microscopy for histological alterations [29].

2.16 Statistical Analysis

The results of the study are expressed as mean ± SEM. The statistical analysis of the data was done using (GraphPad Prism 6, USA). Significant differences were set at *$p < 0.05$ [30].

3 Results and Discussion

3.1 Transmission Electron Microscopy

Size of the bare Fe_3O_4 and Fe_3O_4-PEG NPs as well as their morphology were investigated using TEM as shown in Fig. 1. The Fe_3O_4 NPs showed a size range of 9–20 nm, whereas those coated with PEG had a size range of 5–12 nm, with both particle types demonstrating nearly spherical shapes. However, some of the bare nanoparticles formed aggregates, but they were well dispersed following coating with PEG Fig. 1. Hence, coating with PEG caused a reduction in size and better dispersal of the particles.

3.2 Scanning Electron Microscopy

The size and morphological features of the prepared NPs were further analyzed using scanning electron microscopy. A scanning microscope image of the same batch of samples is demonstrated in Fig. 1 and provides an indication of the achievement of a large quantity of uniform NPs (both bare Fe_3O_4 and Fe_3O_4-PEG), with a mean size of about 14–23 nm for bare Fe_3O_4, and 8–17 nm for Fe_3O_4-PEG. These results demonstrated that the produced NPs were well within the favored size for the purposes for efficient delivery of the harbored drugs, indicating a possible selective absorbance of the PEG surfactant onto the favorable facets of the particles, leading to possible inhibition of the free growth of Fe_3O_4.

Fig. 1 TEM and SEM images of bare Fe_3O_4 and Fe_3O_4-PEG nanoparticles
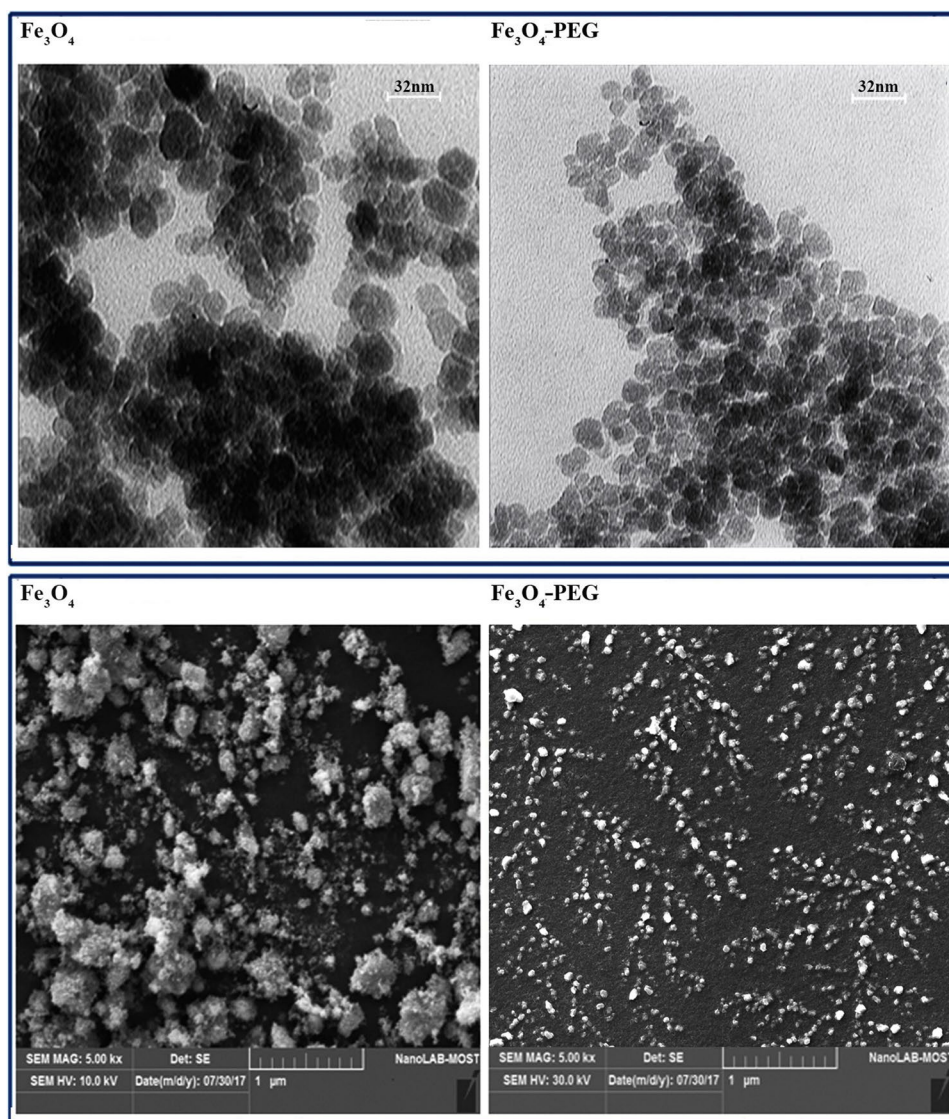
3.3 Structural Characteristics of Bare Fe_3O_4 and PEG-Fe_3O_4

FTIR analysis is essential test for the characterization of the functional groups which is present in bare Fe_3O_4 and PEG-Fe_3O_4NP. The FTIR spectra of bare Fe_3O_4 and PEG-Fe_3O_4NP were recorded in the spectral region 4000–400 cm^{-1}. The FTIR results of the bare Fe_3O_4 and PEG-Fe_3O_4NP samples are shown in Fig. 2 that depicts the FTIR spectra of the Fe_3O_4-PEG and bare Fe_3O_4NPs. As a result of capping of the NPs with PEG, a significant increase was observed in the stretching bands of –CH at 2926 cm^{-1} and –OH at 3338.89 cm^{-1}. The wavenumber 2306.94 and 2311.30 cm^{-1} indicated the presence of alkene (C=C) group. 1896.23 cm^{-1} indicated the presence of anhydride group C=O, 1732.13 and 1730. 21 cm^{-1} refer to the presence of aldehyde group C=O. 1685.84,

and 1687.77 cm^{-1} indicated the presence of conjugated aldehyde C=O. 1608.69, 1610.61 cm^{-1} indicated the presence of C=C α,β-unsaturated ketone group. 1558.54 cm^{-1} demonstrated the presence of N–O stretching belong nitro compound. The bands between 1465.95 to band 1300.07 cm^{-1} indicated the presence of O-H hydroxyl group of carboxylic acid. These data are following those of a previous report [31]. The stretching vibration of the C–C group of PEG was evidenced in the peak absorptions at 1114.89 cm^{-1} (–C–O–C–) and the bond at 1464 cm^{-1} Fig. 2. These peaks confirmed the successful incorporation of PEG onto the NPs. The bands between 986.30 to band 630.74 cm^{-1} indicated the presence of C=C alkene group. The results also demonstrated metal-oxygen bands at 580.59 cm^{-1} and 426 cm^{-1}, which corresponded to intrinsic stretching vibrations of the metal at the tetrahedral (Fetetra–O) and octahedral (Feocta–O) sites.

Fig. 2 FTIR analysis of bare Fe_3O_4 and Fe_3O_4-PEG nanoparticles
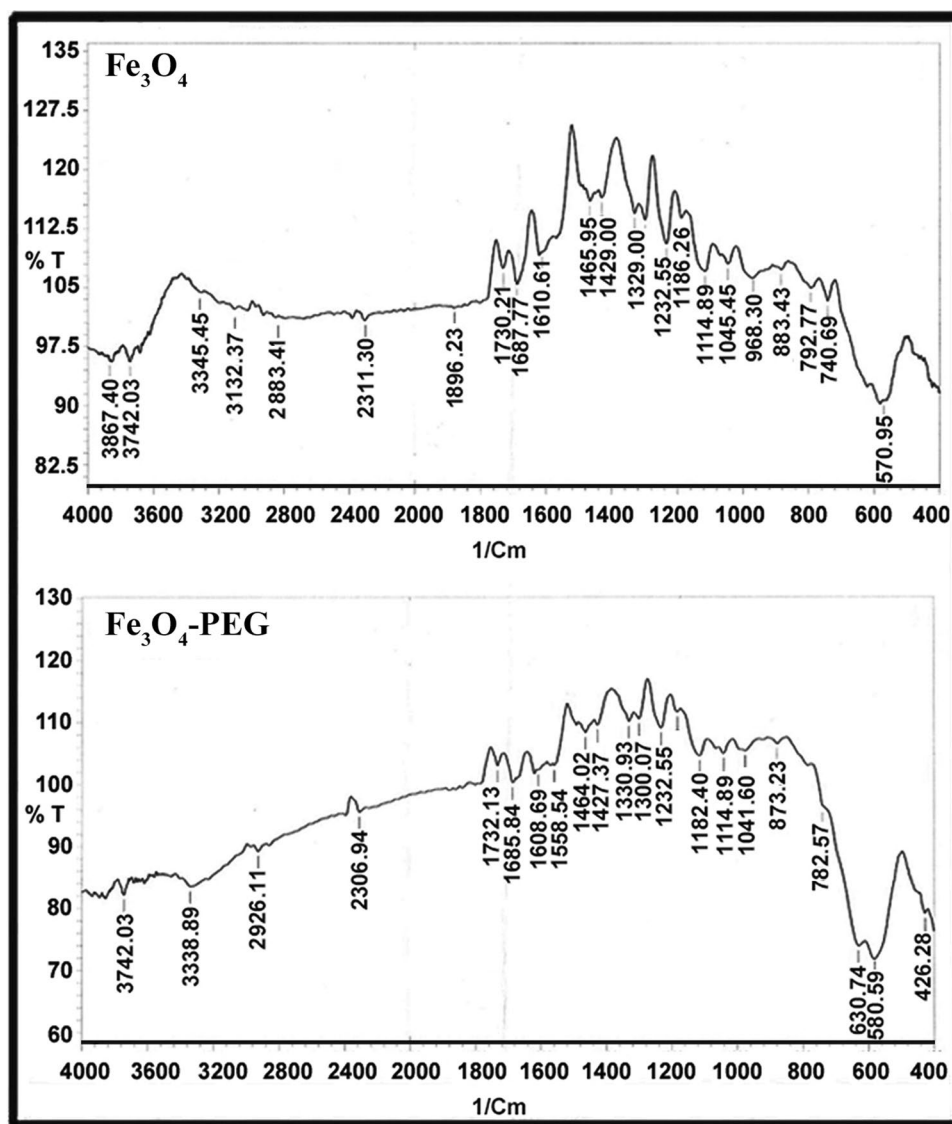
3.4 Bare Fe_3O_4 and Fe_3O_4-PEG Inhibited Cancer Cells Proliferation

In this study, we tested the cytotoxic impact of bare Fe_3O_4 and Fe_3O_4-PEG at different concentrations as indicated in Fig. 3 against AMJ13 (human breast cancer cells), using the MTT assay. The treatment of cells with bare Fe_3O_4 and Fe_3O_4-PEG for 72 h caused a significant reduction in the capacity of cancer cells to proliferate. The data demonstrated the cytotoxic effect of bare Fe_3O_4 and Fe_3O_4-PEG with concentrations of 6.25, 12.5, 25, 50, and 100 µg mL^{-1} against cancer cells in comparison with untreated cells. Moreover, the bare Fe_3O_4 and Fe_3O_4-PEG demonstrated the highest cytotoxic impacts against AMJ13 cells at IC_{50} values was 37.33 µg mL^{-1} for bare Fe_3O_4 and 18.23 µg mL^{-1} for Fe_3O_4-PEG. Taken together, cell viability results proposed a selective mode of the inhibitory impact of the bare Fe_3O_4

and Fe_3O_4-PEG on breast cancer cells. A recent study [32] demonstrated that the anti-cancer activity of Polyvinylpyrrolidone loaded-$MnZnFe_2O_4$ magnetic nanocomposites against AMJ13, MCF-7, and SKOV-3 cell lines is increased when Polyvinylpyrrolidone loaded-MnZnFe2O4 nanocomposites used with NIR laser, while highly increased cytotoxic activities were observed after exposure of Polyvinylpyrrolidone loaded-$MnZnFe_2O_4$ nanocomposites to induction heating with AMF. They are explained one possible mechanism by which Polyvinylpyrrolidone loaded-$MnZnFe_2O_4$ nanocomposites killed cancer cells. Treated cancer cells with polyvinylpyrrolidone loaded-$MnZnFe_2O_4$ magnetic nanocomposites significantly increased ROS synthesis, with subsequent reduction of the MMP. The results their study demonstrated that Polyvinylpyrrolidone loaded-$MnZnFe_2O_4$ nanocomposites suppressed cancers cells' proliferation and has a growth inhibitory effect on different cancer cells, resulting
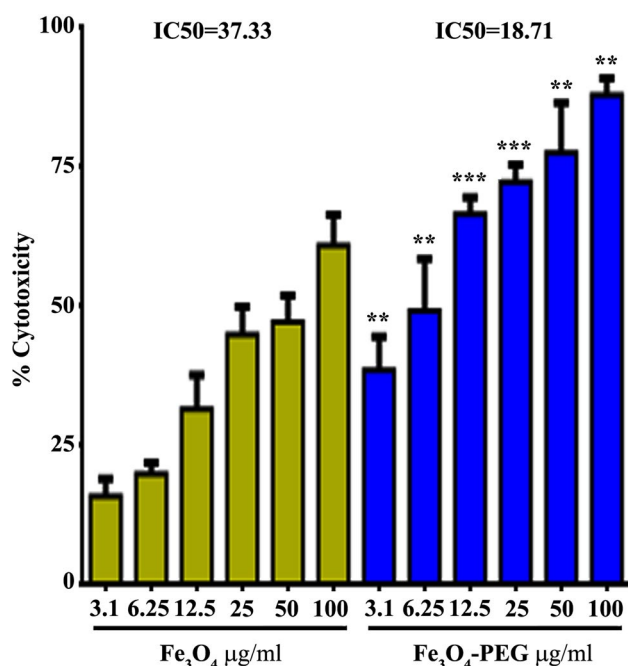
**Fig. 3** Anti-proliferative activity of bare Fe_3O_4 and Fe_3O_4-PEG nanoparticles against AMJ13 cell line. The values are expressed as mean $\pm$ SEM. **$P < 0.01$, ***$P < 0.001$

in apoptosis as a novel pathway that involves mitochondrial damage mechanism via activated P53. Other study [33] demonstrated that the Fe3O4 MNPs are prepared by biosynthesis method using *Sargassum muticum* extract had anti-proliferative activity against various types of cancer cell lines including human cell lines for leukemia (Jurkat cells), breast cancer (MCF-7 cells), cervical cancer (HeLa cells), and liver cancer (HepG2 cells). The tumor cells were treated with different concentrations of Fe3O4 MNPs. The results showed ability of Fe3O4 MNPs to inhibits cancer cells through apoptosis pathway. F@Tyr Fe3O4 NPs were prepared using chemical precipitation method to provide biocompatibility and biofunctionalization. The prepared nanoparticles loaded with chemotherapyTMX. Both nanoparticles and nanoparticles loaded with TMX had cytotoxicity and inhibitory effect against HEK-293 cell line. The results F@Tyr@TMX NPs exhibited more cytotoxic effect than that of free TMX. The main therapeutic advantage of drug loaded nanoparticles in magnetically targeted drug delivery is expected to be more pronounced in In-vivo studies where the efficacy of free drug is negligible [34].

3.5 Estimation of Apoptosis Using AO/PI Dual-Staining

Apoptosis is characterized by specific morphological properties and biochemical reactions that are limited by energy, with pyknosis (condensation of chromatin) and

cell shrinkage being the early hallmarks of the process. Shrinkage of cells occurs because of condensed organelles and densified cytoplasm, while pyknosis is regarded as the most crucial characteristic of the early events of apoptosis [12]. Events associated with late apoptosis are associated with the formation of organelles-containing buds made by extensively blebbed portions of the plasma membrane [13]. In the present study, fluorescence microscopy was used to test for the activities of the bare Fe_3O_4 and Fe_3O_4-PEG in apoptosis induction. Alterations in the morphology of the cancer cells were observed. The untreated cells retained their normal structure (Fig. 4), while the treatment for 24 h caused typical apoptotic events, including shrinkage of the cytoplasm and blebbing of the membrane. Detection of cells with early apoptosis was achieved through the binding of the AO dye to the fragmented DNA, leading to the emission of bright green fluorescence. Following 24 h of treatment with bare Fe_3O_4 and Fe_3O_4-PEG, apoptosis was observed through the occurrence of condensed nuclear chromatin and blebbing (Fig. 4). Also, the same treatment was associated with the late apoptosis events as observed by the appearance of a reddish-orange color due to the binding between ethidium bromide and the denatured DNA. The association between the morphological alterations and apoptosis in the treated mice was time-dependent. In this study, we tested the possibility that inducing apoptosis had a relation to the anti-proliferation events in the breast cancer cells following their treatment with bare Fe_3O_4 and Fe_3O_4-PEG. This was performed via the analysis of the apoptosis-associated events such as the morphological alterations in the nucleus and the fragmentation of DNA. Figure 4 demonstrates the intact morphology of the nucleus in the control cells, while cells treated with bare Fe_3O_4 and Fe_3O_4-PEG displayed chromatin condensation. To confirm our results, the percentage of apoptotic cells was determined by staining the cancer cells with the annexin V-FITC using the flow cytometry. The flow cytometry results showed that the cells undergoing apoptosis were labeled with annexin V at quadrant Q3. Figure 4 shows dot plots of AMJ13 cells treated with bare Fe_3O_4 and Fe_3O_4-PEG nanoparticles for 24 h at IC_{50} concentration. In the untreated AMJ13 cells, the majority (97.2%) of cells were viable and non-apoptotic, and in AMJ13 treated with bare Fe_3O_4 and Fe_3O_4-PEG was a decreased in the viable cells and increased in cells undergoing apoptosis. The percentage of apoptotic cells in the control untreated AMJ13 was 2.64%. While in bare Fe_3O_4 and Fe_3O_4-PEG treated AMJ13 cells the percentage increased to 20.8%, and 30.1% respectively. The increasing percentage of the annexin V^+/PI^+ population indicating dead or necrotic cells was observed when the AMJ13 cells that were treated with bare Fe_3O_4 and Fe_3O_4- PEG. The results investigated
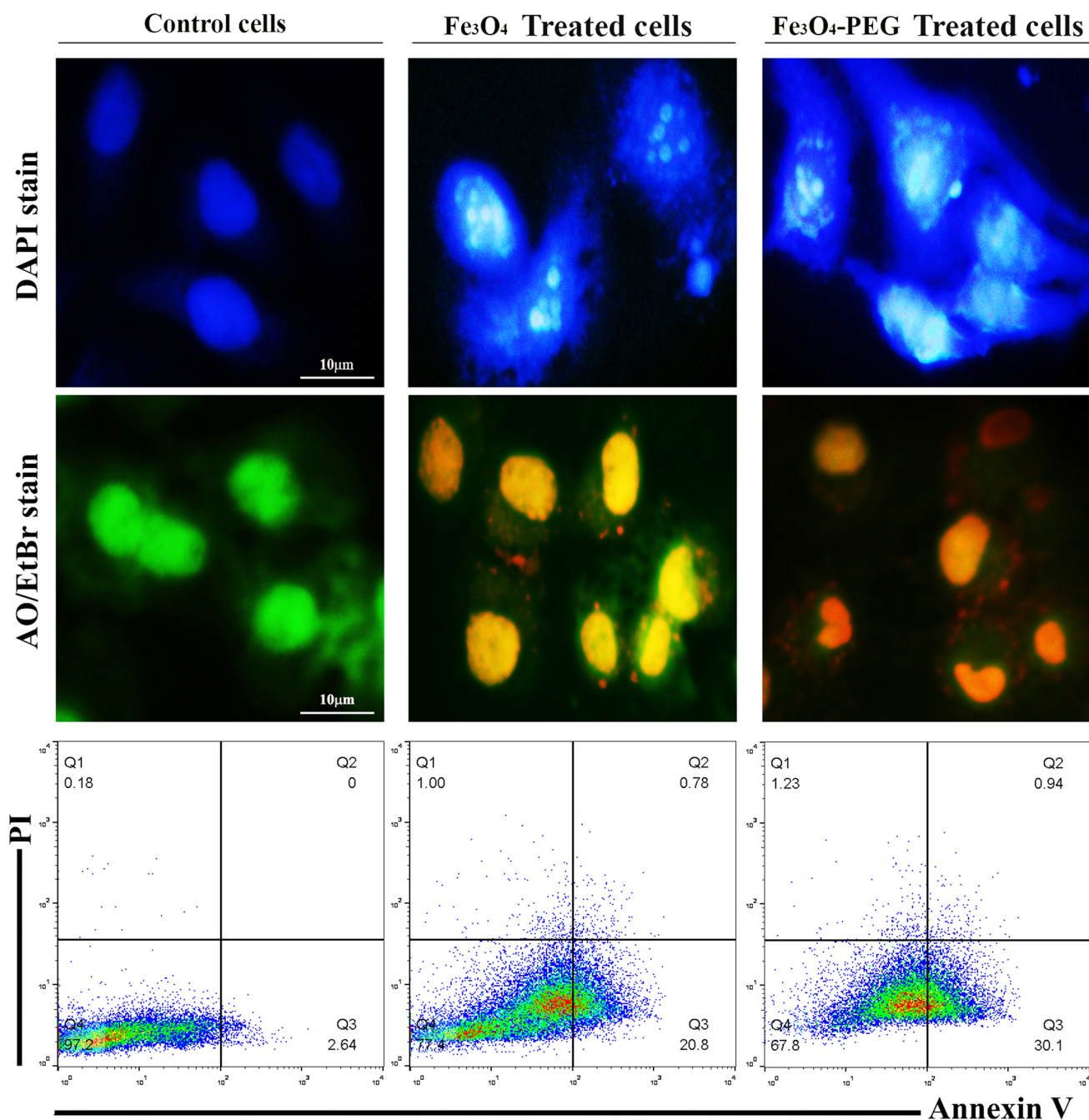
Fig. 4 Apoptosis markers in AMJ13 cells after treatment with bare Fe$_3$O$_4$ and Fe$_3$O$_4$-PEG nanoparticles. The upper panel represented the DNA fragmentation assay. The middle panel represented AO/EtBr assay (Scale bar: 10 μm). The lower panel represented the flow cytometry assay

the high ability of bare Fe$_3$O$_4$ and Fe$_3$O$_4$-PEG to cause damage and induce death to the AMJ13 treated cells cell due to the capability of bare Fe$_3$O$_4$ and Fe$_3$O$_4$-PEG to penetrate through the membrane and make a change on the mRNA expression levels of the genes which play a role in controlling of apoptosis pathways, these genes include p53, Bax, BCL-2, caspase-3, and caspase-9.

3.6 Effect of Bare Fe$_3$O$_4$ and Fe$_3$O$_4$-PEG on Mitochondrial Function

The mitochondria take a fundamental part in the inductive events of apoptosis through different death stimuli. Alterations in the mitochondria involve the disruption of their membrane potential and the release of cytochrome *c* to the cytoplasm, eventually resulting in caspase-3 induction

through mechanisms that depend on caspase-9. Therefore, we investigated the impacts of treatment with bare Fe_3O_4 and Fe_3O_4-PEG on the mitochondrial membrane potential in AMJ13 cells. Following treatment with these two types of NPs, cells were stained with MMP dye and then examined by a fluorescent microscope. This stain has the property of selective entry to the mitochondria, following membrane potential, leading to the production of strong red fluorescence. As shown in Fig. (5a), the treatment with the bare Fe_3O_4 and Fe_3O_4-PEG reduced the proportion of
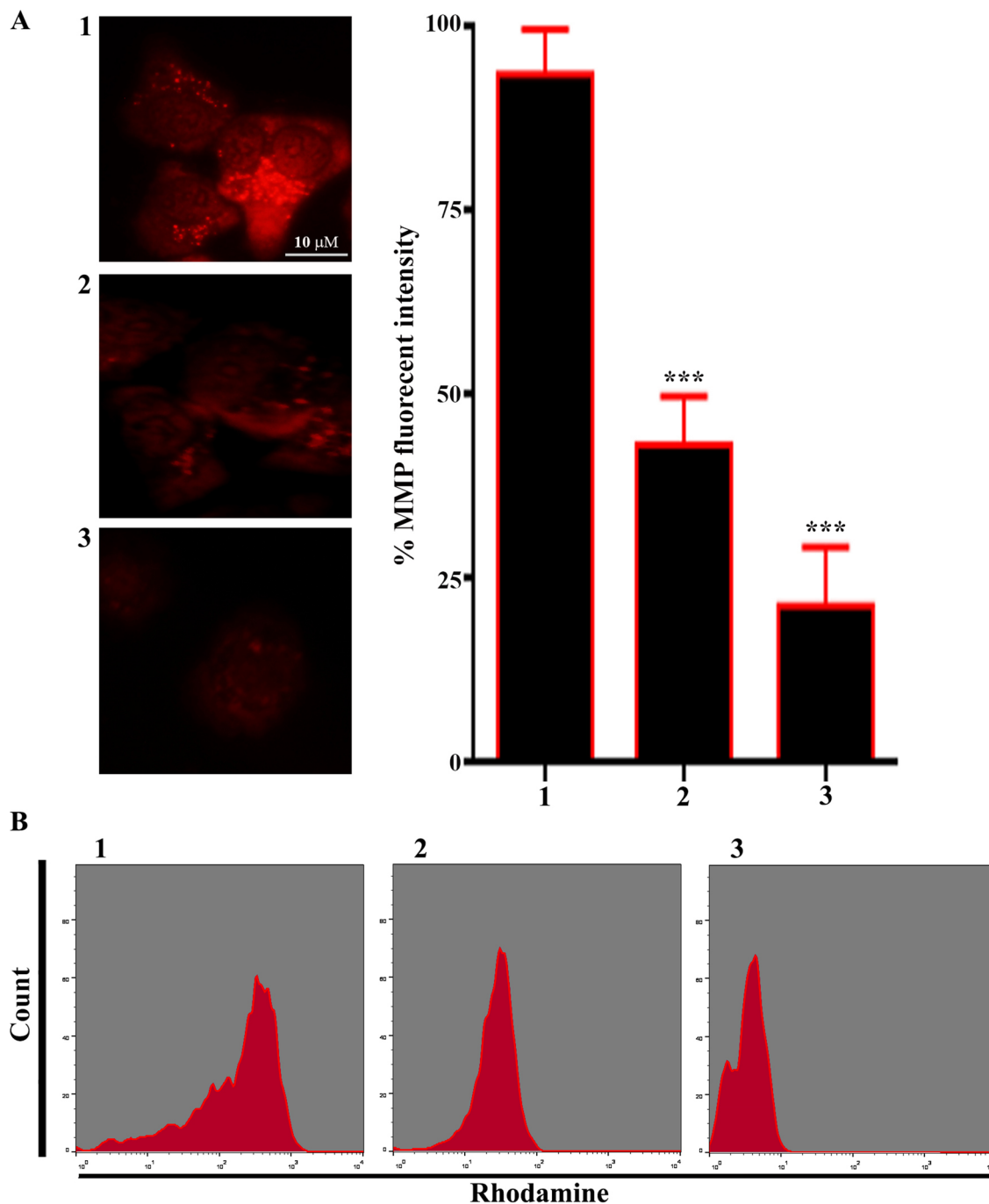
Fig. 5 Dysfunction of MMP in AMJ13 cells after treatment with bare Fe_3O_4 and Fe_3O_4-PEG NPs. **a** The fluorescent intensity of MMP indicator JC 1 in the control untreated AMJ13 cells (1). AMJ13 cells were treated with bare Fe_3O_4 NPs (2). AMJ13 cells were treated with Fe_3O_4_PEG NPs (3) (Scale bar: 10 μm). The graph represents the statistical analysis of the fluorescent intensity ratio. The data are represented as mean ± SEM. ***P < 0.001. **b** Flow cytometry results in AMJ13 cells were treated as indicated in A. Rhodamine stain was used to investigate the loss of mitochondrial membrane potential

red fluorescent cells from 5% in the control to almost 54%, and almost 77% in the cells treated with bare Fe_3O_4 and Fe_3O_4-PEG, respectively. These data demonstrated the involvement of mitochondrial dysfunction in the induction of programmed cell death in AMJ13 cells because of the treatment with bare Fe_3O_4 and Fe_3O_4-PEG. The reduction in mitochondrial membrane potential is a significant and important marker for the apoptotic cell death process. The level of mitochondrial membrane potential was investigated by using the flow cytometric method after staining the cells with Rhodamine (Rh123 probe). We measured the quantity of apoptotic AMJ13 cells after treatment with bare Fe_3O_4 and Fe_3O_4-PEG at IC_{50} concentration. A sizable increase of the dead cells due to the treatment with bare Fe_3O_4 and Fe_3O_4-PEG in AMJ13 cells was demonstrated in Fig. 5b. AMJ13 cells were treated with bare Fe_3O_4 and Fe_3O_4-PEG at IC_{50} for 24 h. The cells showed a high reduction in Rh123 stain that indicates the depletion of mitochondrial membrane potential compared with the control untreated AMJ13 cells.

3.7 Cellular Uptake of Fe_3O_4 and Fe_3O_4-PEG Nanoparticles

The cellular uptake of FITC-labeled bare Fe_3O_4 and Fe_3O_4-PEG in AMJ13 cells was observed by a fluorescent microscope. Nanoparticle uptake was found to be higher in bare Fe_3O_4 and Fe_3O_4-PEG treated cells than in the control cells. Furthermore, the uptake of FITC-labeled bare Fe_3O_4 and Fe_3O_4-PEG was quantified by determining the median fluorescence intensity of the FITC signal as indicated in Fig. 6. This finding demonstrated the uptake, and internalization of FITC-labeled bare Fe_3O_4 and Fe_3O_4-PEG into the AMJ13 cell line. Bare Fe_3O_4 and Fe_3O_4-PEG can cause death and induce apoptosis, due to cell-penetrating ability and capability to bind with the nuclear protein.

3.8 Bare Fe_3O_4 and Fe_3O_4-PEG Induced ROS Generation

Controlled ROS formation is a characteristic feature of living cells with normal function. Uncontrolled elevation in ROS formation occurs upon oxidative stress conditions, leading to disrupted proteins, membrane lipids, and nucleic acid. Oxidative damage accompanies a wide range
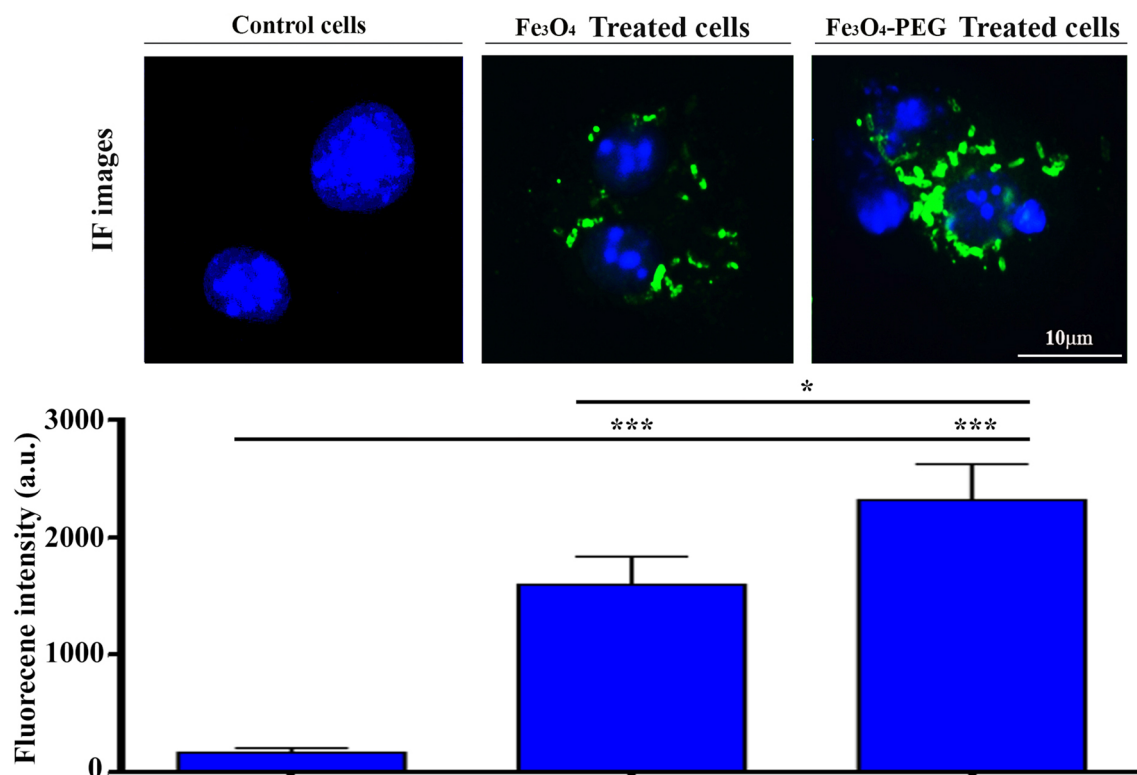
Fig. 6 Cellular uptake of FITC-labeled bare Fe_3O_4 and Fe_3O_4-PEG NPs in AMJ13 cells. Cells were monitored by fluorescence microscopy after 12 h of incubation at 37 °C (Scale bar: 10 μm). The bar graph represents the median fluorescent intensity of the FITC signal detected in AMJ13 cells. Data are represented as mean ± SEM. **P < 0.01, ***P < 0.001

of diseases and conditions such as aging. Research on diseases associated with oxidative stress makes the advantage of critical approaches such as ROS measurement probes. Immediately after H2DCFDA entry into cells, intracellular esterases eliminate acetate groups from H2DCF, which is efficiently reserved within the cells. ROS-mediated oxidation of H2DCF produces fluorescent DCF. The detection of ROS can be performed through the detection of the fluorescence increase using devices such as flow cytometer, fluorometer, microplate reader, or fluorescence microscope, and applying excitation sources and filters that are suitable for fluorescein (FITC). Due to the susceptibility of the stains to photo-oxidation, it is recommended to employ low light settings for fluorescence microscopy. In this study, the results show that the fluorescent intensity of H_2DCF significantly increased after the treatment of the AMJ13 cells with bare Fe_3O_4 and Fe_3O_4-PEG as in Fig. 7.

3.9 Bare Fe_3O_4 and Fe_3O_4-PEG Increased of Bax and Decreased of Bcl-2 Expression

The tight regulation of the events initiated within the mitochondria is achieved via the Bcl-2 protein family, such as those with pro- and anti-apoptotic properties. Progressive or abortive events of apoptosis are regulated via the action of 25 genes expressing for this family. Bax is a protein with pro-apoptosis properties that participates in the liberation of cytochrome c to the cytoplasm through steps of dimerization and trans-membrane translocation. The proteins with anti-apoptosis properties, including Bcl-2, inhibit this translocation process. In this study, the levels of Bcl-2 and Bax were determined by immunofluorescence, and RT-PCR techniques. The data revealed a significant decrease in Bcl-2 level upon the treatment of AMJ13 cells with bare Fe_3O_4 and Fe_3O_4-PEG at concentrations of 37.33 and 18.23 µg mL^{-1} after 24 h, as compared with the control cells (Fig. 8). Nevertheless, Bax expression showed a significant increase following similar treatments. Hence, decreased Bcl-2 and increased Bax expression upon treatment with bare Fe_3O_4 and Fe_3O_4-PEG can result in the disruption of the MMP and, subsequently, the release of cytochrome c and induction of the caspase pathways. Such alterations in the gene expression of Bcl-2 and Bax supports the occurrence of induced apoptosis through a mitochondrial-mediated intrinsic mechanism. In the current study, our results demonstrated that that the expressions of both mRNA and protein levels of

Fig. 7 Bare Fe_3O_4 and Fe_3O_4-PEG nanoparticles induced ROS generation in AMJ13 cells **a** cells untreated as a control. **b** cells were treated with bare Fe_3O_4 NPs. **c** Cells were treated with Fe_3O_4-PEG NPs C (Scale bar: 10 µm). The bar graph represents the median fluorescent intensity of the H_2DCF signal detected in AMJ13 cells. Data are represented as mean ± SEM. ***P < 0.001
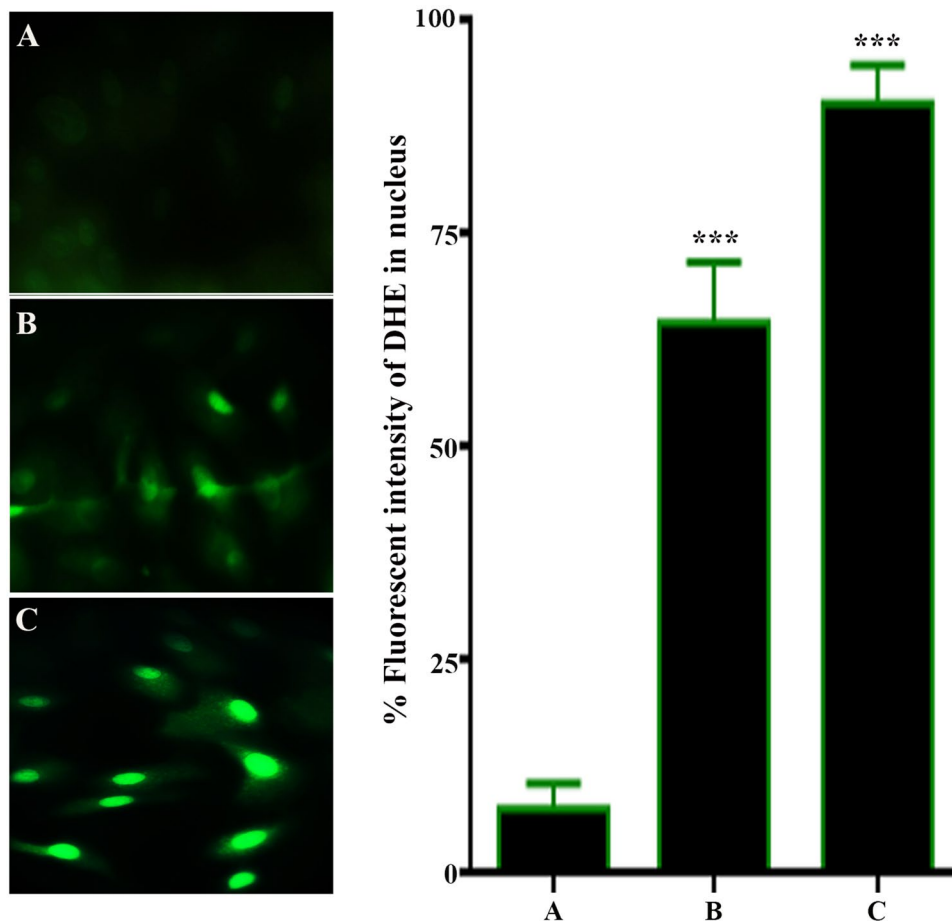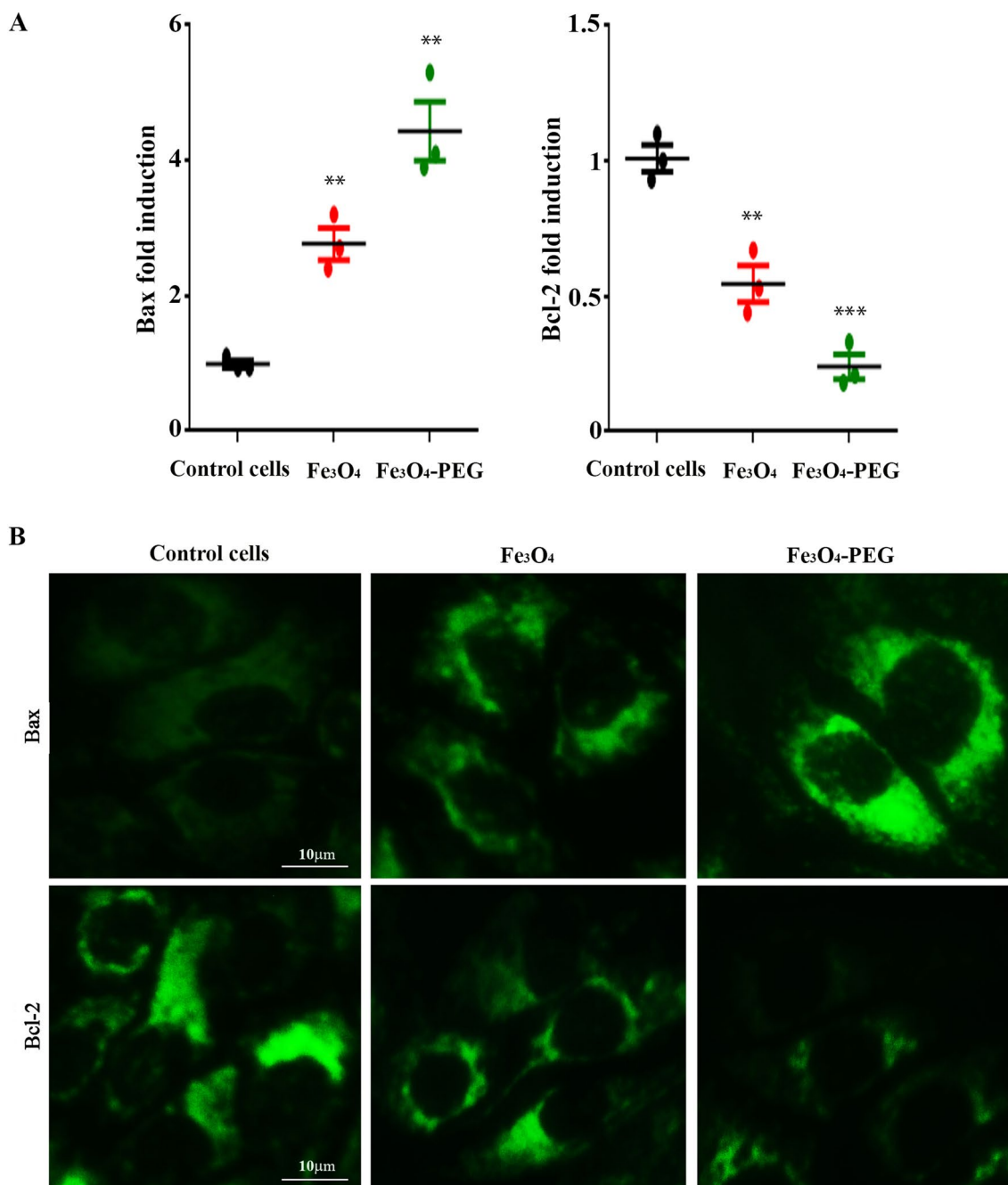
Fig. 8 Bare Fe_3O_4 and Fe_3O_4-PEG nanoparticles up-regulated Bax and down-regulated Bcl-2 genes expression in AMJ13 cells. **a** Graph represents the median of genes expression in AMJ-13 cells after treatment with bare Fe_3O_4 and Fe_3O_4-PEG nanoparticles. The results are represented as mean $\pm$ SEM. **P < 0.01, ***P < 0.001. **b** immunofluorescent assay results of Bax, and Bcl-2 proteins in AMJ13 cells (Scale bar: 10 μm)

apoptotic genes (bax) were upregulated while the expression of antiapoptotic gene bcl-2 was downregulated in AMJ13 cells after treated with bare Fe_3O_4 and Fe_3O_4-PEG at IC50 concentration for 24hr. A previous study by Gopinath et al. [35] have demonstrated that bax is upregulated by p53 pathway. The attachment of bax into the mitochondrial membrane possibly leads to p53-mediated apoptosis. Caspases are activated during apoptosis in many cells and are known to play an important role in both initiation and effecting of apoptosis pathway. Other study was provid that activated caspase-3 is play an important role for cellular DNA damage and apoptosis [36]. Increase and upregulation of p53 leads to activation of proapoptotic members of the bcl-2 family proteins, such as bax, and induces permeabilization

of the outer mitochondrial membrane, which releases soluble proteins from the intermembrane space into the cytosol, where they enhance caspase activation [37]. Once initiated, caspase-9 goes on to activate caspase-3 (effector caspase), which cleaves substrates at aspartate residues, and activation of this proteolytic activity appears to be an event in apoptosis [38].

3.10 NF-κB Translocation was Suppressed by Bare Fe$_3$O$_4$ and Fe$_3$O$_4$-PEG

The suppression of apoptosis by the activity of NF-κB is one of the mechanisms that was reported to contribute to the resistance to cytotoxic therapies [7]. Anticancer agents as well as stress to the cells are among various stimulation sources that are involved in the activation of NF-κB. A linkage was described between these mechanisms and the pathways of extrinsic signaling as well as inducible resistance to the chemical signaling [8]. Therefore, the joint effects of

the inhibition of NF-κB translocation and chemotherapeutic treatment can cause an increase in the effectiveness of cancer treatment. In this study, a fluorescent microscope assay was employed to assess the role of bare Fe$_3$O$_4$ and Fe$_3$O$_4$-PEG in the inhibition of activated NF-κB. In the untreated cells, the elevated fluorescence intensity of NF-κB was found in the cytoplasm of AMJ13 cells in comparison with that intensity in the nucleus as in Fig. 9. After the treatment of AMJ13 cells with bare Fe$_3$O$_4$ and Fe$_3$O$_4$-PEG, a reduction in the fluorescent intensity of NF-κB in the nucleus was observed. The results also showed that the pretreatment of AMJ13 cells with 2 ng mL^{-1} of TNF-α resulted in a raised fluorescence intensity of NF-κB. The present results also showed that treated cells with NPs caused an effective reduction in the activation of the NF-κB signaling pathway in AMJ13 cells as in Fig. 9. They also indicated that the suppression of the translocation of NF-κB could occur because of treated cells with bare Fe$_3$O$_4$ and Fe$_3$O$_4$-PEG, proposing participation of NF-κB suppression events in apoptosis. The novel possible
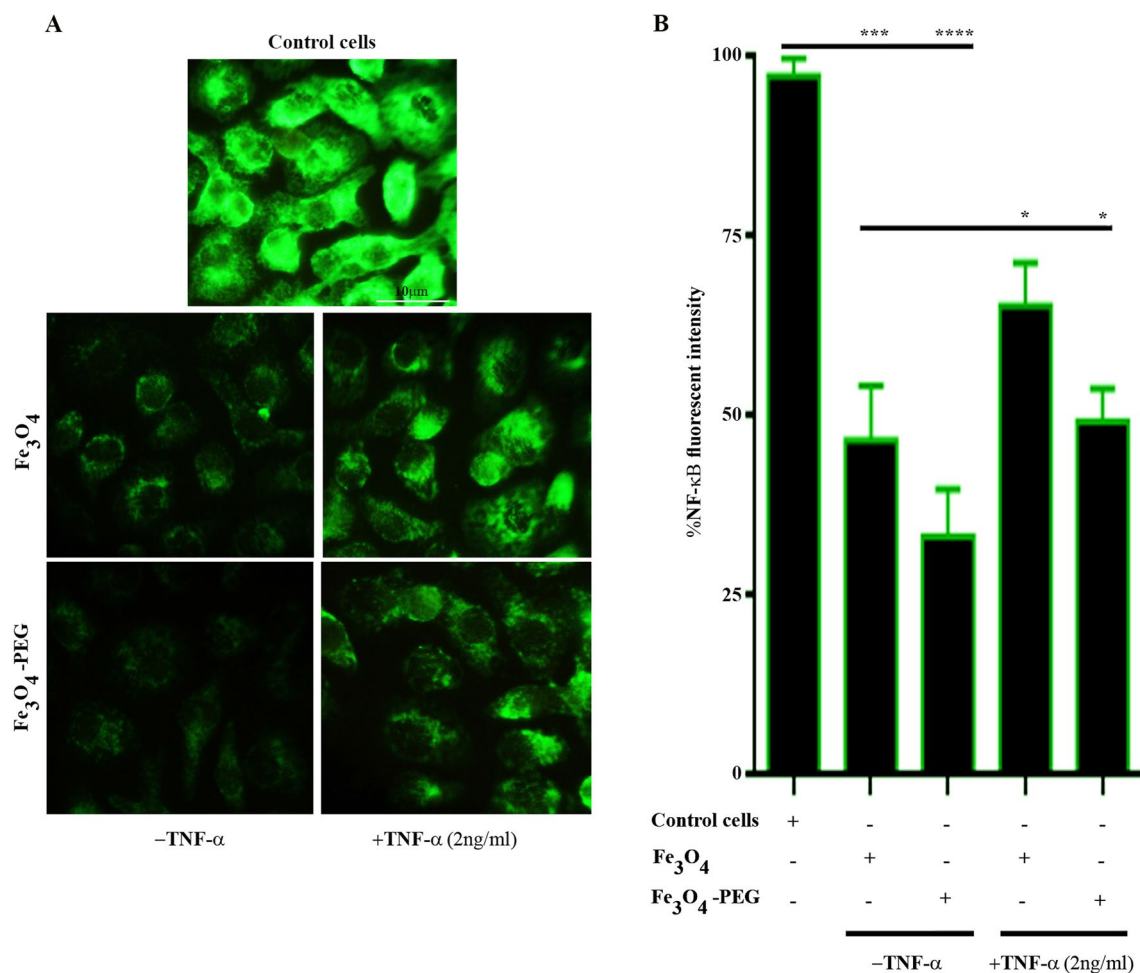
Fig. 9 Bare Fe$_3$O$_4$ and Fe$_3$O$_4$-PEG nanoparticles down-regulated NF-κB activation in AMJ13 cells. **a** immunofluorescent assay results of NF-κB. (Scale bar: 10 μm). **b** Graph represents the median of fluorescence intensity in AMJ-13 cells after treatment with bare Fe$_3$O$_4$ and Fe$_3$O$_4$-PEG nanoparticles. The results are represented as mean ± SEM. *P < 0.05, ***P < 0.001

mechanism by which bare Fe_3O_4 and Fe_3O_4-PEG nanoparticles induce apoptosis in AMJ13 cell line is induction of apoptosis through mitochondrial damage and reduction of NF-κB translocation.

3.11 Measurement Toxicity of Fe_3O_4 and Fe_3O_4-PEG

Blood components such as WBCs, RBCs, and platelets counts were measured before and after treatment with bare Fe_3O_4 and Fe_3O_4-PEG. RBCs counts and shapes were examined using a bright-field microscope, while an immunofluorescent microscope was used to study the effect of the treatment on RBCs fluorescence intensity (Fig. 10). No effects on the body weights of the experimental mice were observed after intraperitoneal injection with Fe_3O_4 and Fe_3O_4-PEG for four weeks (Fig. 11). The serum markers of the kidney functions (urea and creatinine) and liver (GOP,

GPT, and alkaline phosphatase) after intraperitoneal injection of Fe_3O_4 and Fe_3O_4-PEG were measured. No significant differences were recorded in the levels of all these markers when compared to the untreated mice (Fig. 11). The results of this study showed that intraperitoneal injection of Fe_3O_4 and Fe_3O_4-PEG at concentration 500 μg kg^{-1} for 4 weeks did not cause mortality. In addition, differences ($P \leq 0.05$) in body weight between control and injected groups were insignificant. Furthermore, no abnormal clinical signs or behavior was detected between the injected groups and the control mice. Taken together, Fe_3O_4 and Fe_3O_4-PEG at concentration 500 μg kg^{-1} apparently did not cause any toxicity in the animals, while adverse behavioral reactions of different groups were not observed too. Nevertheless, it is still necessary to investigate the toxic effects, including those on body weight, of various administration routes and particle sizes. In the current study,
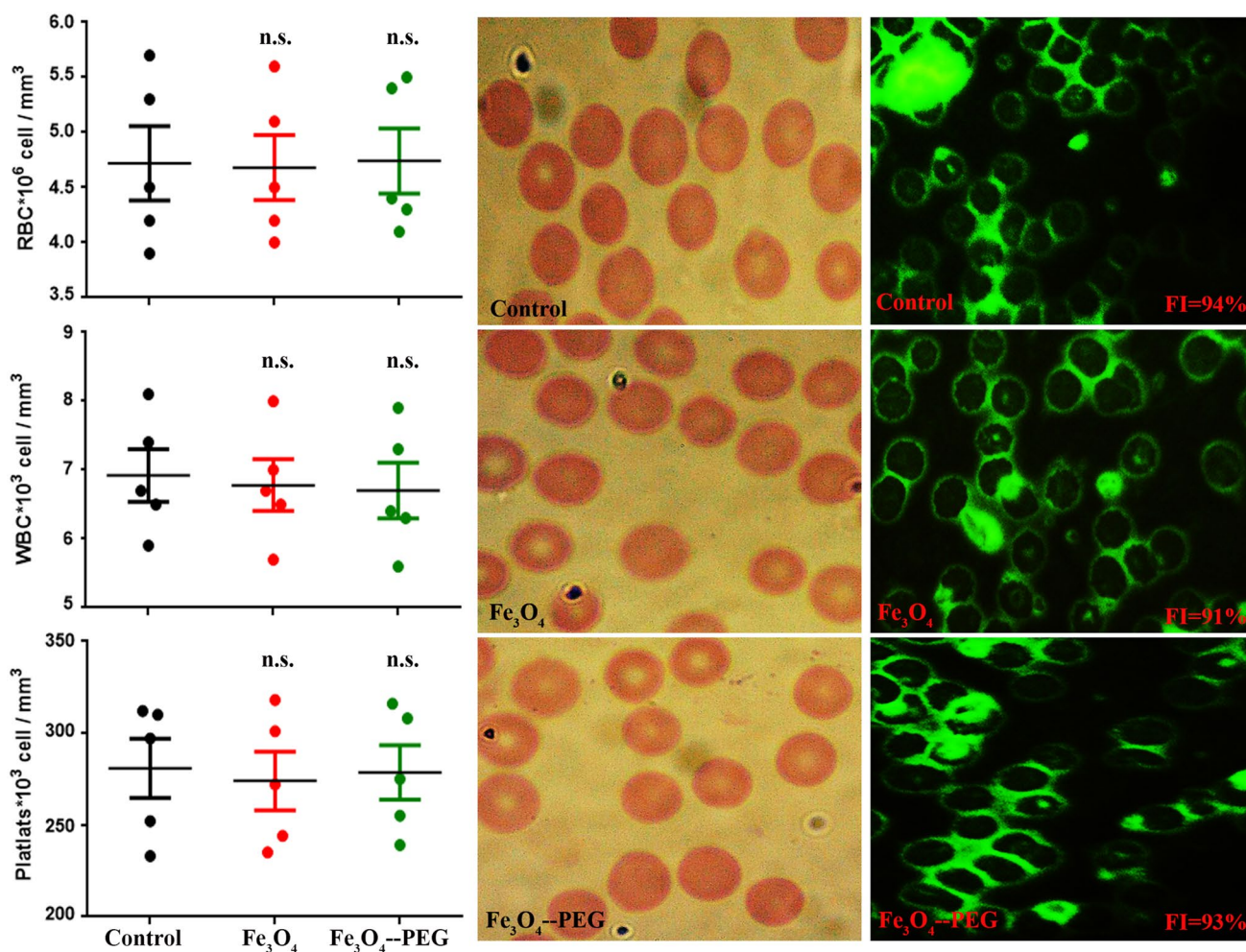
Fig. 10 Effect of bare Fe_3O_4 and Fe_3O_4-PEG NPs in some of the blood components. The graph represents the median of three independent experiments in AMJ-13 cells after treatment with bare Fe_3O_4 and Fe_3O_4-PEG NPs. The results are represented as mean ± SEM. Light microscope photographs of RBCs treated with bare Fe_3O_4 and Fe_3O_4-PEG NPs. Fluorescent intensity of RBCs before and after treatment with bare Fe_3O_4 and Fe_3O_4-PEG NPs
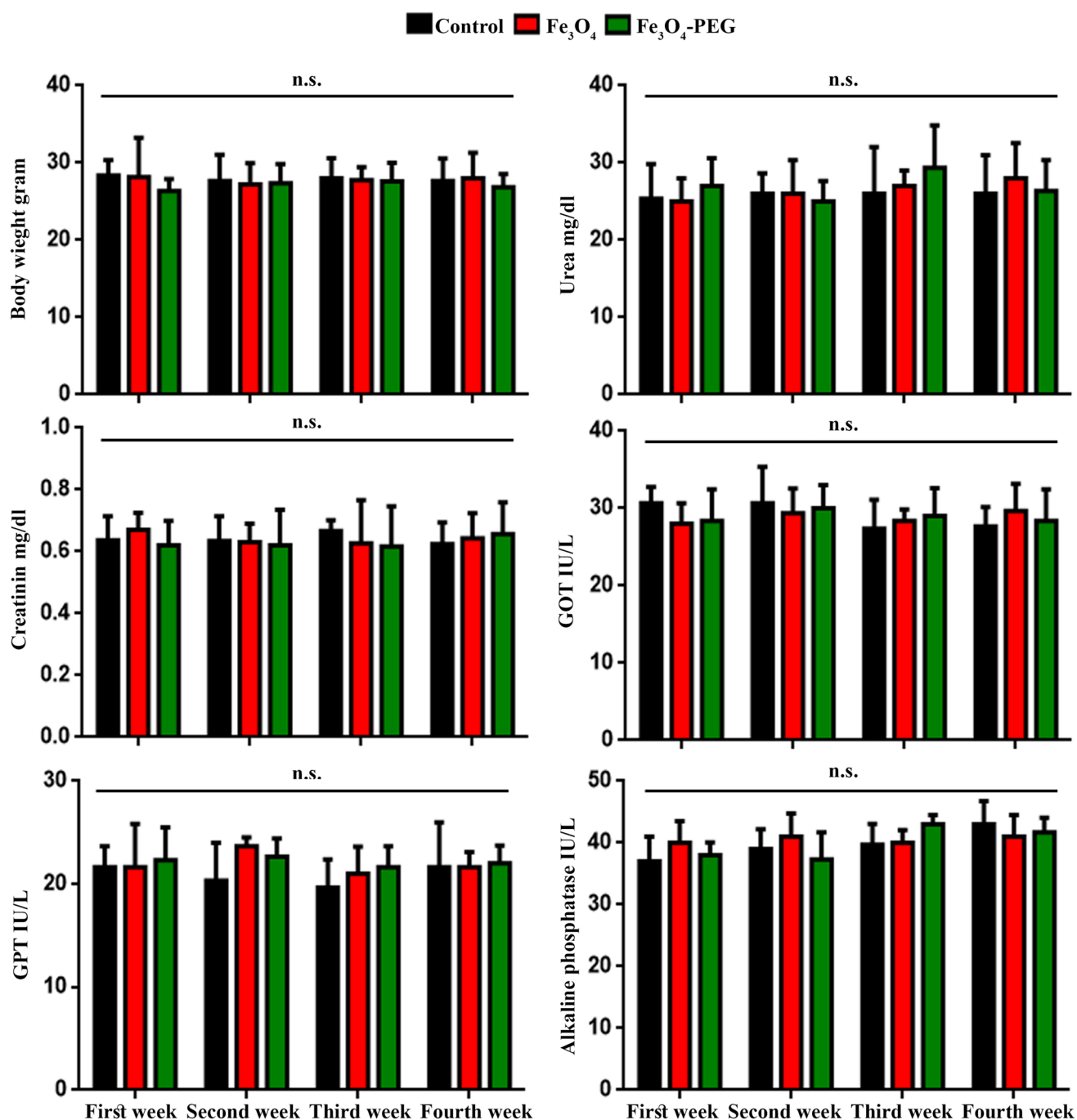
Fig. 11 The in vivo effect of bare Fe_3O_4 and Fe_3O_4-PEG NPs in body weight, urea, creatinine, GPT, GOT, and alkaline phosphatase level of injected mice. The values are expressed as mean $\pm$ SEM. n.s. non-significant

the results of toxic effects in organs such as the liver and kidney were confirmed using biochemical data from the serum of the animals were intraperitoneal injected with bare Fe_3O_4 and Fe_3O_4-PEG mice as well as control group. For liver function test, we are investigated GOP, GPT, and alkaline phosphatase concentration. For kidney function, we measured urea and creatinine level, which is conceder

metabolic products correlated with the functioning of the kidney. For these parameters, the differences caused by the treatment were insignificant ($P \leq 0.05$).. The histopathological tests also demonstrated no significant tissue alterations in the liver, kidneys, and lungs tissues because of bare Fe_3O_4 and Fe_3O_4-PEG (Fig. 12). Our results demonstrated insignificant alterations in the hepatic cords, and
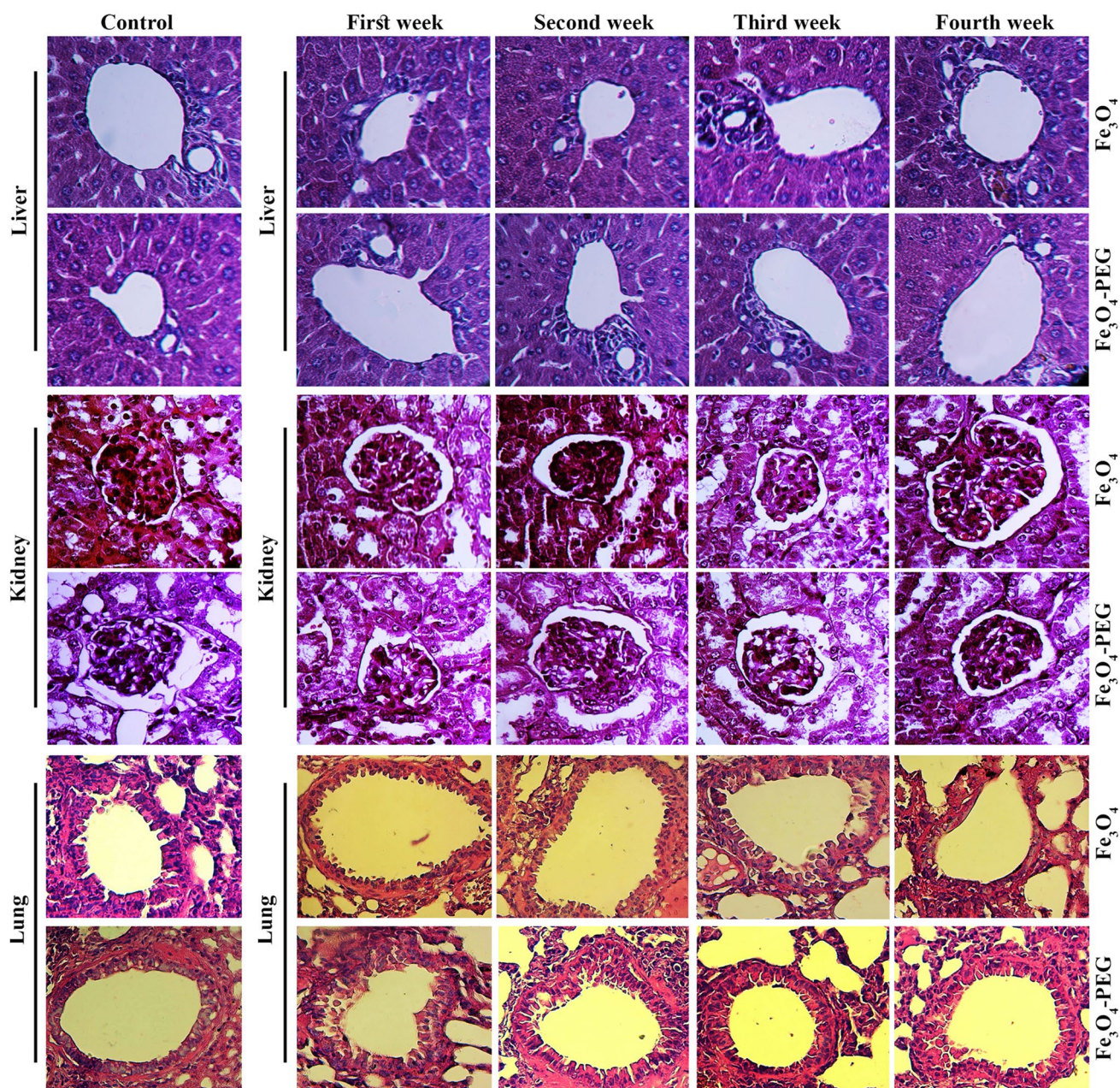
Fig. 12 The in vivo effect of bare Fe_3O_4 and Fe_3O_4-PEG NPs in organs of injected animals. Histopathological sections of liver, kidneys, and lungs in mice after challenged intraperitoneally with bare Fe_3O_4 and Fe_3O_4- PEG NPs. Magnification power 40x

hepatic lobules in the liver of treated mice. The kidney tissues were also similar in the treated and the control groups, as represented by the absence of atrophy of the glomerular and renal tubular epithelial cells. The results also showed no significant alterations in the lung tissues of the treated mice in comparison with the untreated group. Therefore, the exposure of the animals to the bare Fe_3O_4 and Fe_3O_4-PEG did not induce any histopathological alterations in the liver, kidneys, and lungs tissues.

4 Conclusions

In the present Fe_3O_4 nanoparticles were synthesized by hydrothermal method, and coated with the (PEG). The obtained NPs were characterized using different techniques that including SEM, TEM, and FTIR. The results showed that the bare Fe_3O_4 have a mean diameter 9–20 nm, whereas those coated with PEG had a size range

of 5–12 nm. We demonstrated the cytotoxic activity of bare Fe_3O_4 and Fe_3O_4-PEG. The capability of Fe_3O_4-PEG to induce cellular apoptosis was investigated using DAPI, Acridine orange/ Ethedium bromide double stain, flow cytometry to tested mitochondrial membrane potential (MMP), and the production of reactive oxygen species (ROS). RT-PCR, and immunofluorescence were performed to measure expression levels of Bax and Bcl-2 proteins. The side effect of bare Fe_3O_4 and Fe_3O_4-PEG nanoparticles was investigated using animal model.The results demonstrated that nanoparticles were biocompatible for liver, kidney, and lung. The anti-proliferative activity of bare Fe_3O_4 and Fe_3O_4-PEG was associated with the cell cycle arrest as well as the inhibition of NF-κB translocation. The results confirmed the role of intrinsic pathways in the induction of apoptosis in AMJ13 cells.

Compliance with Ethical Standards

Conflict of interest The authors reported no potential conflict of interest.

References

1. F. Bray, J. Ferlay, I. Soerjomataram, R.L. Siegel, L.A. Torre, A. Jemal, Global cancer statistics 2018: Globocan estimates of incidence and mortality worldwide for 36 cancers in 185 countries. CA Cancer J. Clin. **68**, 394–424 (2018)
2. World Health Organization, *Global Health Observatory* (World Health Organization, Geneva, 2018)
3. J.P. Fortin, F. Gazeau, C. Wilhelm, Intracellular heating of living cells through Néel relaxation of magnetic nanoparticles. Eur. Biophys. J. **37**(2), 223–228 (2008)
4. B. Li, M. Shan, X. Di, C. Gong, L. Zhang, Y. Wang, G. Wu, A dual pH-and reduction-responsive anticancer drug delivery system based on PEG–SS–poly (amino acid) block copolymer. RSC Adv. **7**(48), 30242–30249 (2017)
5. S. Naqvi, M. Samim, A.K. Dinda, Z. Iqbal, S. Telagoanker, G.J. Ahmed, A. Maitra, Impact of magnetic nanoparticles in biomedical applications. Recent Pat. Drug Deliv. Formul. **3**(2), 153–161 (2009)
6. T.J. Yu, P.H. Li, T.W. Tseng, Y.C. Chen, Multifunctional Fe_3O_4/ alumina core/shell MNPs as photothermal agents for targeted hyperthermia of nosocomial and antibiotic-resistant bacteria. Nanomedicine **6**, 53–63 (2011)
7. L. Kong, N.F. Rosli, H.L. Chia, J. Guan, M. Pumera, Self-propelled autonomous Mg/Pt janus micromotor interaction with human cells. Bull. Chem. Soc. Jpn. **92**(10), 1754–1758 (2019)
8. Y. Liu, P. Bhattarai, Z. Dai, X. Chen, Photothermal therapy and photoacoustic imaging via nanotheranostics in fighting cancer. Chem. Soc. Rev. **48**(7), 2053–2108 (2019)
9. K. Omri, N. Alonizan, Effects of ZnO/Mn concentration on the micro-structure and optical properties of ZnO/Mn–TiO_2 nanocomposite for applications in photo-catalysis. J. Inorg. Organomet. Polym. Mater. **29**(1), 203–212 (2019)
10. S. Gouadria, Z.M. Elqahtani, F.F. Alharbi, K. Omri, Pyrolysis effect on physical properties of carbon–silica nanocomposites elaborated by sol–gel method. J. Inorg. Organomet. Polym. Mater. (2020)
11. H. Mansour, K. Omri, R. Bargougui, S. Ammar, Novel α-Fe2O3/ TiO2 nanocomposites with enhanced photocatalytic activity. Appl. Phys. A **126**(3), 151 (2020)
12. S.S. Kim, H.J. Cho, J.Y. Kang, H.K. Kang, T.K. Yoo, Inhibition of androgen receptor expression with small interfering RNA enhances cancer cell apoptosis by suppressing survival factors in androgen insensitive, late stage LNCaP cells. Sci World J. **8** (2013)
13. M. Ocker, M. Höpfner, Apoptosis-modulating drugs for improved cancer therapy. Eur. Surg. Res. **48**(3), 111–120 (2012)
14. P.T. Schumacker, Reactive oxygen species in cancer cells: live by the sword, die by the sword. Cancer Cell **10**(3), 175–176 (2006)
15. H.K. Fam, K. Choi, L. Fougner, C.J. Lim, C.F. Boerkoel, Reactive oxygen species stress increases accumulation of tyrosyl-DNA phsosphodiesterase 1 within mitochondria. Sci. Rep. **8**(1), 1–14 (2018)
16. J.C. Martinou, R.J. Youle, Mitochondria in apoptosis: Bcl-2 family members and mitochondrial dynamics. Dev. Cell **21**(1), 92–101 (2011)
17. M. Wierzbicki, E. Sawosz, B. Strojny, S. Jaworski, M. Grodzik, A. Chwalibog, NF-κB-related decrease of glioma angiogenic potential by graphite nanoparticles and graphene oxide nanoplatelets. Sci. Rep. **8**(1), 1–9 (2018)
18. H. Peng, S. Tang, Y. Tian, R. Zheng, L. Zhou, W. Yang, Highly ligand-directed and size-dependent photothermal properties of magnetite particles. Particle Syst. Charact. **33**(6), 332–340 (2016)
19. S. Albukhaty, H. Naderi-Manesh, T. Tiraihi, M. Sakhi Jabir, Poly-l-lysine-coated superparamagnetic nanoparticles: a novel method for the transfection of pro-BDNF into neural stem cells. Artif. Cell Nanomed. Biotechnol. **46**(3), 125–132 (2018)
20. K.S. Khashan, G.M. Sulaiman, S.A. Hussain, T.R. Marzoog, M.S. Jabir, Synthesis, characterization and evaluation of anti-bacterial, anti-parasitic and anti-cancer activities of aluminum-doped zinc oxide nanoparticles. J. Inorg. Organomet. Polym. Mater. (2020). https://doi.org/10.1007/s10904-020-01522-9
21. K.S. Khashan, M.S. Jabir, F.A. Abdulameer, Carbon nanoparticles decorated with cupric oxide nanoparticles prepared by laser ablation in liquid as an antibacterial therapeutic agent. Mater. Res. Exp. **5**(3), 035003 (2018)
22. M.S. Jabir, U.M. Nayef, W.K.A. Kadhim, Polyethylene glycol-functionalized magnetic (Fe3O4) nanoparticles: a novel DNA-mediated antibacterial agent. Nano Biomed Eng, **11**(1) (2019)
23. G.M. Sulaiman, H.M. Waheeb, M.S. Jabir, S.H. Khazaal, Y.H. Dewir, Y. Naidoo, Hesperidin loaded on gold nanoparticles as a drug delivery system for a successful biocompatible, anti-cancer, anti-inflammatory and phagocytosis inducer model. Sci. Rep. **10**(1), 1–16 (2020)
24. H.N.K. AlSalman, E.T. Ali, M. Jabir, G.M. Sulaiman, S.A. AlJadaan, 2BenzhydrylsulfinylNhydroxyacetamideNa extracted from fig as a novel cytotoxic and apoptosis inducer in SKOV3 and AMJ13 cell lines via P53 and caspase8 pathway. Eur. Food Res. Technol. 2020

25. H.A. Kadhem, S.A. Ibraheem, M.S. Jabir, A.A. Kadhim, Z.J. Taqi, M.D. Florin, Zinc oxide nanoparticles induces apoptosis in human breast cancer cells via caspase-8 and *P53* pathway. Nano Biomed. Eng. **11**(1), 35–43 (2019)

26. M.S. Jabir, U.M. Nayef, W.K. Abdulkadhim, G.M. Sulaiman, Supermagnetic Fe3O4-PEG nanoparticles combined with NIR laser and alternating magnetic field as potent anti-cancer agent against human ovarian cancer cells. Mater. Res. Exp. **6**(11), 115412 (2019)

27. I.I.J. Alsaedi, Z.J. Taqi, A.M. Abdul Hussien, G.M. Sulaiman, M.S. Jabir, Graphene nanoparticles induces apoptosis in mcf-7 cells through mitochondrial damage and nf-kb pathway. Mater. Res. Exp. **6**(9), 095413 (2019)

28. C. Coman, F. Tabaran, I. Ilie, Assessment of silver nanoparticles toxicity in human red blood cells using ELISA and immunofluorescence microscopy techniques. Biotechnol. Mol. Biol. Nanomed. **1**, 61–65 (2013)

29. I.H. Ali, M.S. Jabir, H.S. Al-Shmgani, G.M. Sulaiman, A.H. Sadoon, Pathological And immunological study on infection with *Escherichia coli* in ale balb/c mice. J. Phys. **1003**(1), 12009 (2018)

30. Z. Ali, M. Jabir, A. Al-Shammari, Gold nanoparticles inhibiting proliferation of Human breast cancer cell line. Res. J. Biotechnol. **14**, 79–82 (2019)

31. W.K.A. Kadhim, U.M. Nayef, M.S. Jabir, Polyethylene glycol-functionalized magnetic (Fe_3O_4) nanoparticles: a good method for a successful antibacterial therapeutic agent via damage DNA molecule. Surf. Rev. Lett. **26**(10), 1950079 (2019)

32. S.H. Kareem, A.M. Naji, Z.J. Taqi, M.S. Jabir, Polyvinylpyrrolidone loaded-MnZnFe2O4 magnetic nanocomposites induce apoptosis in cancer cells through mitochondrial damage and P53 pathway. J. Inorg. Organomet. Polym. Mater. (2020). https://doi.org/10.1007/s10904-020-01651-1

33. F. Namvar, H.S. Rahman, R. Mohamad, J. Baharara, M. Mahdavi, E. Amini et al., Cytotoxic effect of magnetic iron oxide nanoparticles synthesized via seaweed aqueous extract. Int. J. Nanomed. **9**, 2479 (2014)

34. H. Nosrati, N. Rashidi, H. Danafar, H.K. Manjili, Anticancer activity of tamoxifen loaded tyrosine decorated biocompatible Fe 3 O 4 magnetic nanoparticles against breast cancer cell lines. J. Inorg. Organomet. Polym Mater. **28**(3), 1178–1186 (2018)

35. P. Gopinath, S.K. Gogoi, P. Sanpui, A. Paul, A. Chattopadhyay, S.S. Ghosh, Signaling gene cascade in silver nanoparticle induced apoptosis. Colloids Surf. B **77**(2), 240–245 (2010)

36. R.U. Janicke, M.L. Sprengart, M.R. Wati, A.G. Porter, Caspase-3 is required for DNA fragmentation and morphological changes associated with apoptosis. J. Biol. Chem. **273**(16), 9357–9360 (1998)

37. P. Fuentes-Prior, G.S. Salvesen, The protein structures that shape caspase activity, specificity, activation and inhibition. J. Biochem. **384**(Pt 2), 201–232 (2004)

38. R.J. Youle, A. Strasser, The BCL-2 protein family: opposing activities that mediate cell death. Nat. Rev. Mol. Cell Biol. **9**(1), 47–59 (2008)

Publisher's Note Springer Nature remains neutral with regard to jurisdictional claims in published maps and institutional affiliations.